ADVANCED FUNCTIONAL MATERIALS
www.afm-journal.de

Accurate Extraction of Charge Carrier Mobility in 4-Probe Field-Effect Transistors

Hyun Ho Choi, Yaroslav I. Rodionov, Alexandra F. Paterson, Julianna Panidi, Danila Saranin, Nikolai Kharlamov, Sergei I. Didenko, Thomas D. Anthopoulos, Kilwon Cho, and Vitaly Podzorov**

Charge carrier mobility is an important characteristic of organic field-effect transistors (OFETs) and other semiconductor devices. However, accurate mobility determination in FETs is frequently compromised by issues related to Schottky-barrier contact resistance, that can be efficiently addressed by measurements in 4-probe/Hall-bar contact geometry. Here, it is shown that this technique, widely used in materials science, can still lead to significant mobility overestimation due to longitudinal channel shunting caused by voltage probes in 4-probe structures. This effect is investigated numerically and experimentally in specially designed multiterminal OFETs based on optimized novel organic-semiconductor blends and bulk single crystals. Numerical simulations reveal that 4-probe FETs with long but narrow channels and wide voltage probes are especially prone to channel shunting, that can lead to mobilities overestimated by as much as 350%. In addition, the first Hall effect measurements in blended OFETs are reported and how Hall mobility can be affected by channel shunting is shown. As a solution to this problem, a numerical correction factor is introduced that can be used to obtain much more accurate experimental mobilities. This methodology is relevant to characterization of a variety of materials, including organic semiconductors, inorganic oxides, monolayer materials, as well as carbon nanotube and semiconductor nanocrystal arrays.

1. Introduction

Charge carrier mobility, μ, is an important parameter in organic and inorganic semiconductor field-effect transistors (FETs).[1] Achieving higher mobilities has been one of the primary research objectives particularly in organic electronics, where molecular synthesis, interface engineering, or blending different organic semiconductors allows creating a very broad range of new materials and devices with greatly varied μ.[2] In this situation, it becomes critically important to develop standardized methods for error-free characterization of mobility in novel FETs. Unambiguous determination of μ from FET measurements may not be as straightforward as it appears from the standard FET equations (that is, Shockley-style equations relating the source–drain current, I_{SD}, in the transistor's channel with the gate and source–drain voltages, V_G and V_{SD}).[3,4] These equations, routinely used by researchers for the analysis of FETs, are derived under several assumptions, also known as the gradual channel approximation model (see ref. [3] and Ch. 2.2 in ref. [5]), including: a) carrier mobility μ is independent of the carrier density n, b) longitudinal electric field being much smaller than the gate electric field, and c) a negligible contact resistance. The latter aspect, the contact resistance, is especially important in devices based on undoped band insulators (such as, e.g., organic semiconductors[6]) or high

Dr. H. H. Choi, Prof. V. Podzorov
Department of Physics
Rutgers University
Piscataway, NJ 08854, USA
E-mail: podzorov@physics.rutgers.edu
Dr. H. H. Choi, Prof. K. Cho
Department of Chemical Engineering and Center for Advanced Soft Electronics
Pohang University of Science and Technology (POSTECH)
Pohang 37673, South Korea
E-mail: kwcho@postech.ac.kr
Prof. Y. I. Rodionov, Dr. D. Saranin, Dr. N. Kharlamov, Prof. S. I. Didenko, Prof. V. Podzorov
Department of Semiconductor Electronics and Semiconductor Physics
National University of Science and Technology "MISiS"
Moscow 119049, Russia
Prof. Y. I. Rodionov
Institute for Theoretical and Applied Electrodynamics RAS
Moscow 125412, Russia
Dr. A. F. Paterson, Prof. T. D. Anthopoulos
Physical Sciences and Engineering Division (PSE)
King Abdullah University of Science and Technology (KAUST)
Thuwal 23955-6900, Saudi Arabia
J. Panidi, Prof. T. D. Anthopoulos
Department of Physics and Centre for Plastic Electronics
Imperial College London
South Kensington
London SW7 2AZ, UK

DOI: 10.1002/adfm.201707105

mobility–gapped semiconductors (such as, e.g., transition metal dichalcogenides[7]), where a Schottky barrier is typically formed at the metal–semiconductor interface, leading to a substantial contact resistance.[6,8,9] It can lead, for instance, to a type of nonlinearity in $I_{SD}(V_G)$ characteristics in FETs, called a "hump," presenting as a local steep upturn of I_{SD} near the transistor's onset and leading to erroneous mobility claims in literature.[2]

One of the most efficient methods of addressing contact resistance in semiconductor devices is to perform 4-probe measurements. In organic electronics, these measurements were introduced with the advent of high-quality single-crystal organic field-effect transistors (OFETs).[5,10–13] In these measurement, two (or more) electrodes are added in the channel, in addition to the usual source and drain contacts, and a potential drop, V_{4p}, along the corresponding section of the channel is measured between these voltage probes during the FET's operation (for details, see Ch. 2.1 of ref. [5]) (**Figure 1**). Usually, voltage probes are added symmetrically (two on either side of the channel, as shown in Figure 1a), because such a structure can also be used for Hall effect measurements.[14–23] Here, we consider this "symmetric" type of 4-probe geometry. In 4-probe FETs, the source–drain current and 4-probe voltage are simultaneously measured as functions of gate voltage, $I_{SD}(V_G)$ and $V_{4p}(V_G)$, and used in the extraction of a contact-corrected 4-probe mobility, μ_{4p}, and contact resistance.[10,11] Because a fraction of the net source–drain voltage, V_{SD}, is dropped across the resistive Schottky barriers, μ_{4p} is typically greater than or equal to the 2-probe carrier mobility, μ_{2p} ($\mu_{4p}/\mu_{2p} \geq 1$).

In addition to the regular (that is, longitudinal) FET measurements, contact resistance can also affect measurements of Hall mobility, μ_H, because in Hall effect measurements, the longitudinal 4-probe channel conductivity, σ_{4p}, is used in a combination with the Hall carrier density, n_H, to determine the Hall mobility as $\mu_H \equiv \sigma_{4p}/(en_H)$, where e is the electron charge.[19] Thus, using the contact-corrected 4-probe conductivity, σ_{4p} is also important for Hall effect studies. In turn, comparing the correctly extracted longitudinal (4-probe) and Hall carrier mobilities, μ_{4p} and μ_H, is very important for materials' characterization, as it helps elucidating the fundamental charge transport mechanisms in newly developed OFETs, especially important in cases of mobilities in the range 0.1–10 $cm^2\ V^{-1}\ s^{-1}$, when band-like and hopping carriers may coexist.[19] Thus, given the overwhelming importance of 4-probe and Hall measurements for material development and characterization, it would be very important to address the specific pitfall of these measurements that we call here the longitudinal channel shunting effect.

Ideal 4-probe structures should use point-like voltage probes to minimize perturbation of the electric field and potential distributions in the channel. However, practical limitations of feature size in shadow masks and lithographically defined contacts may lead to substantial widths of the voltage probes in actual devices (Figure 1) that could result in a reduced gradient of potential (a weaker electric field) in the sections of the channel immediately adjacent to the equipotential edges of the voltage probes and, correspondingly, to a higher potential drop (a stronger electric field) elsewhere in the channel. In this work, we show theoretically and experimentally that such a longitudinal channel shunting can lead to a substantial overestimation of the charge carrier mobility in conventional 4-probe measurements (that is, measurements assuming point-like voltage probes) and its variants. Moreover, we show that longitudinal channel shunting can be a source of error in Hall mobility measurements as well. Based on our numerical simulations of the electric potential and electric field distributions in FETs' channel, we show that one can convert inaccurate experimental 4-probe mobilities, μ_{4p}, to a corrected for shunting mobility, $\mu_{4p\text{-}corr}$, by simply using a correction factor α that depends on two geometric parameters: the ratio of the channel length to channel width, L/W, and the ratio of the width of the voltage probes to the center-to-center distance between them, t/D.

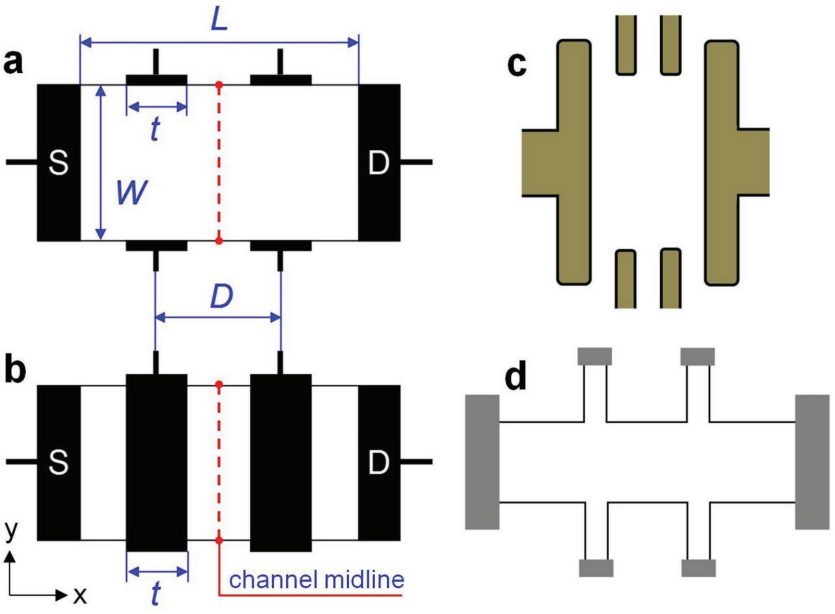

Figure 1. Common 4-probe contact geometries used in organic or inorganic FETs and other devices. a) The conventional 4-probe geometry. The channel length L, width W, the center-to-center distance between the voltage probes D, and their width t are defined in the sketch. The 4-probe voltage, V_{4p}, and the Hall voltage, V_H, are measured between the two voltage probes along and across the channel (in the longitudinal and transverse directions), respectively. b) A limiting case of the standard 4-probe geometry, the so-called "ultimate shunting geometry," in which the voltage probes run across the entire channel, thus completely shunting the two areas of combined width $2t$. Two representative 4-probe contact geometries used in FETs: c) a wide but short channel (L = 200 μm, W = 300 μm, D = 80 μm, t = 35 μm), and d) an elongated channel (L = 260 μm, W = 68 μm, D = 90 μm, and t = 20 μm). In both of these geometries, the voltage probes split the channel in three approximately equal segments of length $D \approx L/3$. The upper bounds of the 4-probe μ overestimation in these two structures are 78% and 30% (above the correct values) for panels (c) and (d), respectively (Equation (3)).

2. The Mobility Overestimation in the Limit of "Ultimate Shunting" Geometry

The conventional 4-probe/Hall-bar contact geometry is shown in Figure 1a: the voltage probes of width t are contacting the channel on each side, thus somewhat shunting the nearest regions of the channel. Let us first consider the structure with the voltage probes deposited throughout the entire width of the channel, the so-called "ultimate shunting" geometry (Figure 1b). In this case, the potential drop along the segments of the channel covered by the metallic voltage probes is assumed to be zero. It would be useful to consider this geometry first, because it corresponds to the strongest shunting and thus represents the limiting case of mobility overestimation. Also, this geometry is actually used in many cases of elongated samples of very small widths, such as nanowires, nanotubes, as well as nano- or microribbons.[24] In conventional 4-probe analysis, the contact-corrected mobility μ_{4p} is found by applying the following equation to the experimental $I_{SD}(V_G)$ and $V_{4p}(V_G)$ dependences[10,11]

$$\mu_{4p} = \left(\frac{1}{C_i}\right)\cdot\left(\frac{D}{W}\right)\cdot\frac{\partial\left(I_{SD}/V_{4p}\right)}{\partial V_G} \quad (1)$$

where C_i is the gate–channel capacitance of a FET. This equation implicitly assumes that the longitudinal electric field in the channel is $E_x = V_{4p}/D$ (x indicates the longitudinal component of the field), which is inaccurate, given the shunting effect. A more precise equation should use the actual longitudinal electric field in the region between the voltage probes, which in the case of an ultimate shunting is $E_x = V_{4p}/(D - t)$, because the net source–drain voltage applied to the channel is dropped only along the part of the channel of length $L - 2t$ (Figure 1b).

By definition, the longitudinal channel conductivity at location x along the channel is $\sigma \equiv \langle j_x\rangle/\langle E_x\rangle = (I_{SD}/W)/\langle E_x\rangle$, where the longitudinal components of the current density j_x (in A cm^{-1}) and electric field E_x are averaged over the channel width at that location (for instance, along the channel's midline shown with the dashed line in Figure 1). That is, $\langle j_x\rangle \equiv I_{SD}/W$, and $\langle E_x\rangle \equiv \frac{1}{W}\cdot\int_{-W/2}^{W/2} E_x(y)\mathrm{d}y$. In the simple case of ultimate shunting (Figure 1b), the local electric field in the channel is not a function of y (we neglect fringe electric fields outside of the channel area), and thus there is no need to average it (but this will be required in a more precise model considered later). Thus, the 4-probe channel conductivity corrected for shunting, $\sigma_{4p\text{-corr}}$, in the ultimate shunting geometry is

$$\sigma_{4p\text{-corr}} \equiv en\mu_{4p\text{-corr}} = \left(\frac{I_{SD}}{V_{4p}}\right)\cdot\left(\frac{D-t}{W}\right) \quad (2)$$

where the charge density in the channel is set by the gate voltage, $en = C_i\cdot(V_G - V_T)$ (V_T is the threshold voltage), and $\mu_{4p\text{-corr}}$ is the 4-probe mobility corrected for longitudinal shunting. By taking the derivative of Equation (2) with respect to V_G, $\mu_{4p\text{-corr}}$ can be expressed via the conventional μ_{4p} as

$$\mu_{4p\text{-corr}} = \left(\frac{1}{C_i}\right)\cdot\left(\frac{D-t}{W}\right)\cdot\frac{\partial(I_{SD}/V_{4p})}{\partial V_G} = (1 - t/D)\cdot\mu_{4p} = \alpha^{-1}\cdot\mu_{4p} \quad (3)$$

The parameter $\alpha \equiv (1 - t/D)^{-1} > 1$ is the correction factor showing by how much μ_{4p} overestimates the actual 4-probe channel mobility $\mu_{4p\text{-corr}}$. Equation (3) shows that 4-probe mobility corrected for shunting, $\mu_{4p\text{-corr}}$, is always lower than conventional 4-probe mobility, μ_{4p}, by $(t/D) \times 100\%$, but becomes equal to it for point-like voltage probes.

The 2-probe mobility, μ_{2p}, more commonly used in FET characterization is also going to be affected by the presence of voltage probes in the channel. The conventional linear-regime 2-probe mobility, μ_{2p}, is extracted in FETs as

$$\mu_{2p} = \left(\frac{1}{C_i\cdot V_{SD}}\right)\cdot\left(\frac{L}{W}\right)\cdot\frac{\partial I_{SD}}{\partial V_G} \quad (4)$$

Here, the source of error is also rooted in the assumption that the longitudinal electric field in the channel is $E_x = V_{SD}/L$ (neglecting the contact resistance). A more precise equation (in the ultimate shunting case of Figure 1b) should use the effective channel length $L - 2t$, and thus the correct electric field is $E_x = V_{SD}/(L - 2t)$, leading to the 2-probe mobility corrected for shunting, $\mu_{2p\text{-corr}}$.

$$\mu_{2p\text{-corr}} = \left(\frac{1}{C_i V_{SD}}\right)\cdot\left(\frac{L-2t}{W}\right)\cdot\left(\frac{\partial I_{SD}}{\partial V_G}\right) = (1 - 2t/L)\cdot\mu_{2p} \quad (5)$$

Equation (5) shows that the 2-probe mobility corrected for shunting $\mu_{2p\text{-corr}}$ is lower than the conventional uncorrected mobility μ_{2p} by up to $(2t/L) \times 100\%$.

Comparison of 4-probe and 2-probe mobilities is indicative of the severity of contact resistance problem in FETs. For instance, $\mu_{4p}/\mu_{2p} = 1$ corresponds to the negligible relative contact resistance, while $\mu_{4p}/\mu_{2p} > 1$ would suggest a non-negligible contact resistance. By dividing Equation (3) by Equation (5), we can evaluate the ratio μ_{4p}/μ_{2p} in conventional measurements and in the shunt-corrected model.

$$\frac{\mu_{4p\text{-corr}}}{\mu_{2p\text{-corr}}} \equiv k\cdot\frac{\mu_{4p}}{\mu_{2p}} = \frac{(1 - t/D)}{(1 - 2t/L)}\cdot\frac{\mu_{4p}}{\mu_{2p}} \quad (6)$$

Note that when the interprobe distance D is smaller than 50% of the channel length ($D/L < 0.5$), the prefactor is $k < 1$, indicating that conventional (not corrected for shunting) measurements would signal an exaggerated severity of the contact resistance problem. On the contrary, for the structures with $D/L > 0.5$, the prefactor is $k > 1$, and thus conventional measurements would underestimate the severity of the contact resistance problem. For instance, if a FET with $D/L > 0.5$ is measured, and the ratio of conventional mobilities is $\mu_{4p}/\mu_{2p} \approx 1$, one might misinterpret the contact quality of such a FET as excellent, while in fact the ratio of the shunt-corrected mobilities in this case would actually be $\mu_{4p\text{-corr}}/\mu_{2p\text{-corr}} > 1$, indicating the presence of a contact problem. When the distance between the voltage probes is exactly 50% of the channel length ($D/L = 0.5$), the prefactor in Equation (6) is $k \equiv 1$, which shows that in such a geometry, the severity of the contact resistance problem can be evaluated correctly, irrespective of the voltage probe width t and the type of measurements.

Equation (6) also reveals an additional very important potential pitfall of 4-probe measurements, occurring when channel shunting is not taken into account. It is easy to see that conventional 4-probe mobility is diverging as $\mu_{4p} = const. \times \frac{(1-2t/L)}{(1-t/D)}$, when the distance D between the voltage probes is reduced, while all the other quantities (including μ_{2p}, $\mu_{4p\text{-corr}}$, and $\mu_{2p\text{-corr}}$) remain constant. In the limiting case of $D \to t$, $\mu_{4p} \to \infty$, which simply corresponds to the voltage probes making a contact with each other, thus resulting in $V_{4p} \to 0$. This shows that by using a 4-probe geometry with a very small distance D between the voltage probes (approaching t), one can obtain an arbitrarily high 4-probe carrier mobility, which would clearly be a gross overestimation of the actual charge carrier mobility of the system. The same artifact may also occur in the more realistic 4-probe contact geometry shown in Figure 1a.

Longitudinal channel shunting could also lead to errors in mobility in Hall effect measurements, because extraction of Hall mobility, μ_H, relies on both the longitudinal 4-probe channel conductivity, σ_{4p}, and Hall carrier density, n_H.

$$\mu_H \equiv \sigma_{4p}/en_H = \left(\frac{1}{B}\right)\cdot\left(\frac{V_H}{V_{4p}}\right)\cdot\left(\frac{D}{W}\right) \tag{7}$$

where V_H is the Hall voltage, B is the magnetic field, and $en_H = I_{SD}B/V_H$.[14,16,19] The longitudinal channel conductivity can be overestimated due to the shunting effect. If one uses the shunt-corrected channel conductivity, $\sigma_{4p\text{-corr}}$ (Equation (2)), the corrected Hall mobility would be:

$$\begin{aligned}\mu_{H\text{-corr}} \equiv \sigma_{4p\text{-corr}}/en_H &= \left(\frac{1}{B}\right)\cdot\left(\frac{V_H}{V_{4p}}\right)\cdot\left(\frac{D}{W}\right)\cdot(1-t/D) \\ &= (1-t/D)\cdot\mu_H = \alpha^{-1}\cdot\mu_H\end{aligned} \tag{8}$$

The analogous Equations (3) and (8) show that in the ultimate shunting limit, both the longitudinal 4-probe mobility and Hall mobility (μ_{4p} and μ_H) are overestimated, and the correction factor is the same: $\alpha = (1 - t/D)^{-1}$. We must caution though that since Hall effect measurements in the ultimate shunting geometry (Figure 1b) are not possible, Equation (8) merely represents a cursory estimate for the upper bound of Hall mobility overestimation in practical Hall-bar geometries due to the use of an overestimated channel conductivity σ_{4p}. For a better evaluation of the shunt-corrected Hall mobility $\mu_{H\text{-corr}}$, one needs to use the more precise computational model described below that uses the conventional realistic Hall-bar geometry (Figure 1a). In addition to corrections in σ_{4p}, we are yet to consider the effect of a reduced longitudinal electric field in the region between the Hall probes that should lead to a reduced Lorentz force acting on charge carriers in the vicinity of those probes in the geometry shown in Figure 1a. This effect can lead to an overestimated n_H. Therefore, these two factors (overestimated σ_{4p} and n_H) may partially compensate each other in the calculation of Hall mobility by the conventional Equation (7), resulting in a smaller degree of error in Hall mobility measurements, compared to that in the longitudinal 4-probe FET mobility.

The model described thus far, although representing merely a limiting case of channel shunting, shows that popular 4-probe FET geometries can easily lead to a serious overestimation of mobility. For instance, when voltage probe width is ≈44% of the distance between the probes ($t = 0.44 \times D$), as in the exemplary channel geometry shown in Figure 1c, this would result in the conventional 4-probe mobility $\mu_{4p} = \mu_{4p\text{-corr}} \times \frac{D}{D-t} = 1.78 \times \mu_{4p\text{-corr}}$. Of course, in conventional 4-probe structures (Figure 1a), the overestimation will be somewhat smaller, and the correction factor α will be a function of L/W and t/D, because the actual distribution of electric field in the channel and the lowering of the potential gradient near the voltage probes will depend on the channel geometry.

3. Numerical Corrections to μ in Conventional 4-Probe/Hall-Bar Contact Geometry

In practical devices for FET measurements and other transport studies, voltage probes should ideally contact the rectangular channel only on the sides, without protruding into the channel, as shown in Figure 1a. The structures with voltage probes significantly protruding into the channel are close to the ultimate shunting geometry shown in Figure 1b and would result in a much more severe mobility overestimation (Equations (3) and (5)). To quantitatively describe the shunting effect in the conventional 4-probe/Hall-bar structure shown in Figure 1a, one needs to numerically solve the full electrostatic problem for a specific channel geometry defined by dimensions L, W, D, and t, with realistic boundary conditions. The numerical results for mobility overestimation, or the parameter $\alpha \equiv \mu_{4p}/\mu_{4p\text{-corr}}$, will then depend on the ratios L/W and t/D. Here, we have performed such numerical simulations for the most common structure (with the voltage probes dividing the channel in three equal sections, $D = L/3$) and for a range of channel geometries (L/W = 0.5–9.1 and t/D = 0–0.85) by solving the Laplacian equation for the electric potential (for details on device simulations, see Figure S1 and the given text in the Supporting Information).

Figure 2 shows the numerical solution for the electric potential and electric field distributions in the channel. It can be clearly seen that the electric potential $\varphi(x, y)$ is greatly affected by the presence of the metallic voltage probes (Figure 2a). In particular, the gradient $\partial\varphi/\partial x$ along the channel is noticeably reduced in the area between the Hall probes V_1 and V_1' (or V_2 and V_2'). The fine arrows in Figure 2b represent the distribution of the local in-plane electric field $E(x, y)$ in the channel for two cases, t/D = 0.06 and 0.6. It is clear that for the structure with wide voltage probes (on the right), E in the area between the Hall probes is reduced more significantly than in the structure with narrow voltage probes (on the left). Panel (c) shows the computed longitudinal component of the electric field E_x as a function of the position y in the transverse direction (along the channel width) at the channel's midline ($x = L/2$), revealing that $E_{x=L/2}$ increases toward the edges of the channel. This effect appears to be the result of a partial termination of the electric field lines at the equipotential edges of the voltage probes, meaning that some current density sinks into these electrodes, but the same amount of current density flows out of them. The net contribution of the

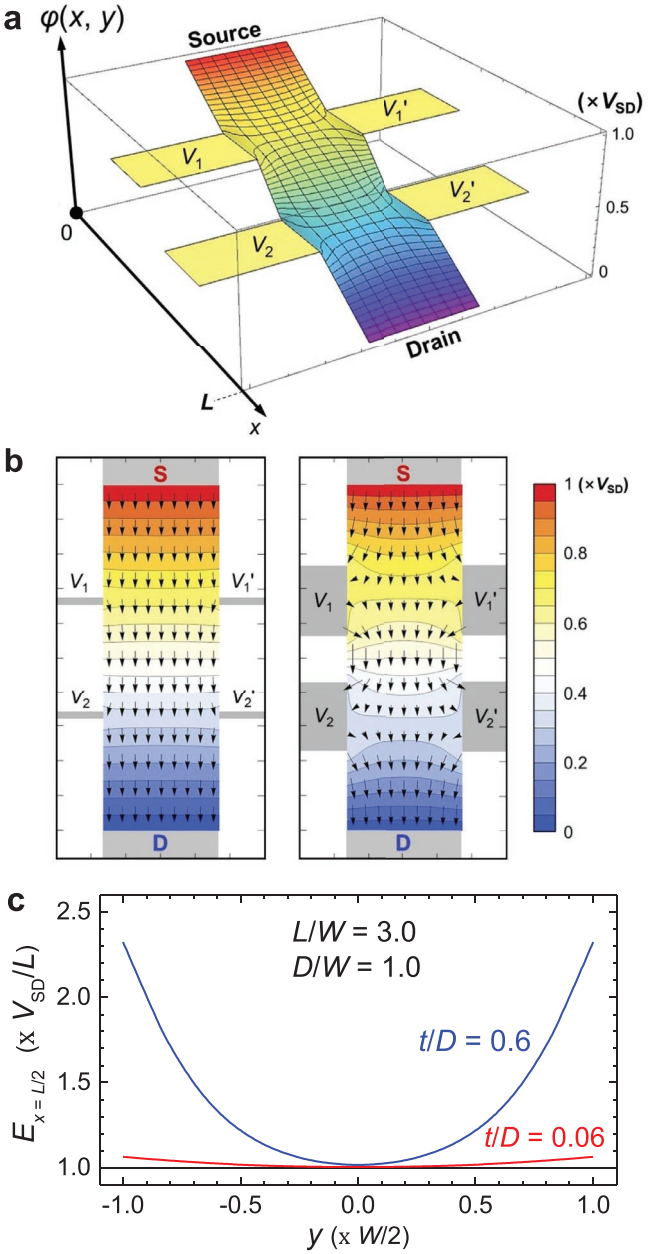

Figure 2. Numerical simulations of the electric potential and longitudinal electric field distributions in FETs' channel in 4-probe/Hall-bar contact geometry. $\varphi(x, y)$ and $E(x, y)$ are computed in the presence of a pair of metallic voltage probes contacting the channel on each side (structure in Figure 1a). In these simulations, W and t are varied in the range 11–50 and 2–28 arbitrary units (a.u.), respectively, while L is fixed at 100 a.u., and D is fixed at $L/3$. V_{SD} input is 100 a.u., so that V_{SD}/L is 1. a) An example of 3D potential surface $\varphi(x, y)$ with equipotential lines, showing that the gradient in the longitudinal direction $\partial\varphi/\partial x$ is reduced between the Hall probes (labeled V_1, V_1', and V_2, V_2') and enhanced in other areas of the channel. b) Calculated local electric field $E(x, y)$ is shown by the arrows for two representative cases: (left) narrow voltage probes with $t = 2$ a.u., and (c) very wide voltage probes with $t = 20$ a.u. c) The computed distribution of the longitudinal component of electric field at the channel midline, $E_{x=L/2}(y)$, along the channel width, $-W/2 < y < W/2$.

voltage probes to the total current in the channel is, of course, zero, because the voltage probes are assumed to be connected to an ideal voltmeter with infinite input resistance.

Using these numerical simulations, we have calculated the average (over the channel width) longitudinal component of the electric field, $\langle E_x \rangle$, at the channel's midline (that is, along the dashed line in Figure 1a at $x = L/2$): $\langle E_x \rangle_{\text{midline}} \equiv \frac{1}{W} \cdot \int_{-W/2}^{W/2} E_x(y)\mathrm{d}y$.

The mobility extracted from the experiments is inversely proportional to the assumed longitudinal electric field in the channel, $\mu \propto E_x^{-1}$, and thus the correction parameter α, showing by what factor the conventional 4-probe mobility overestimates the actual mobility, is

$$\alpha \equiv \frac{\mu_{4p}}{\mu_{4p\text{-corr}}} = \frac{\langle E_x \rangle_{\text{midline}}}{(V_{4p}/D)} \tag{9}$$

We emphasize that in our numerical simulations, neither $\langle E_x \rangle_{\text{midline}}$ nor V_{4p}/D is fixed, but both are computed as functions of L/W and t/D parameters (Supporting Information).

Figure 3 shows the correction factor α calculated for a range of t/D and L/W values (for the geometry with an even division of the channel by the voltage probes, $D = L/3$). It clearly shows the tendency for α to increase with both t/D and L/W, which is expected from the physics of shunting. Indeed, the wider the voltage probes, the greater the portion of the channel that is shunted, thus leading to a stronger mobility overestimation. Also, the greater the L/W ratio (the channel elongation), the closer on average charge carriers are to the equipotential edges of the Hall probes while passing between them, thus becoming more affected by shunting. It is clear from Figure 3 that if shunting is not taken into account, the conventional 4-probe mobility, μ_{4p}, could be

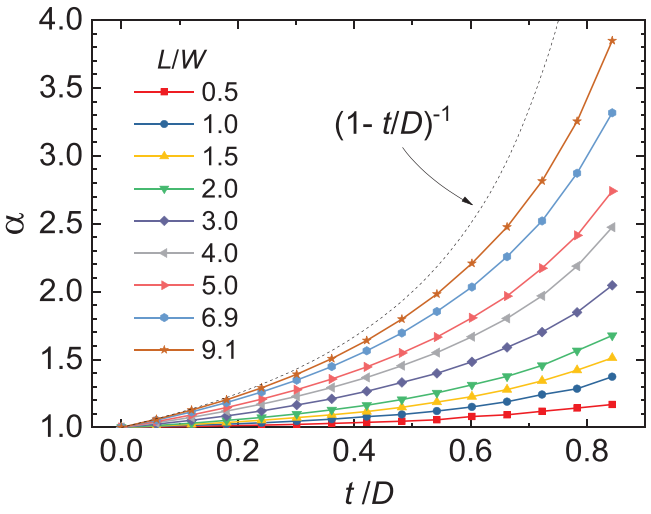

Figure 3. Numerically computed correction factor $\alpha \equiv \mu_{4p}/\mu_{4p\text{-corr}}$ for 4-probe/Hall-bar contact geometry shown in Figure 1a. α is given by the ratio of the average longitudinal electric field at the midline position in the channel ($x = L/2$) to the longitudinal electric field assumed in conventional 4-probe measurements (Equation (9)). The horizontal axis is the relative width of the voltage probes, t/D. The aspect ratio of the channel L/W is used as parameter (indicated). D is fixed at $L/3$. The dashed curve corresponds to parameter α in the ultimate shunting limit (Equation (3)). These calculations show that in devices with elongated channels and wide voltage probes, μ_{4p} can be significantly overestimated by up to a few hundred percent. For a zoom-in on the crowded portion of this data set at low t/D, see Figure S2 (Supporting Information).

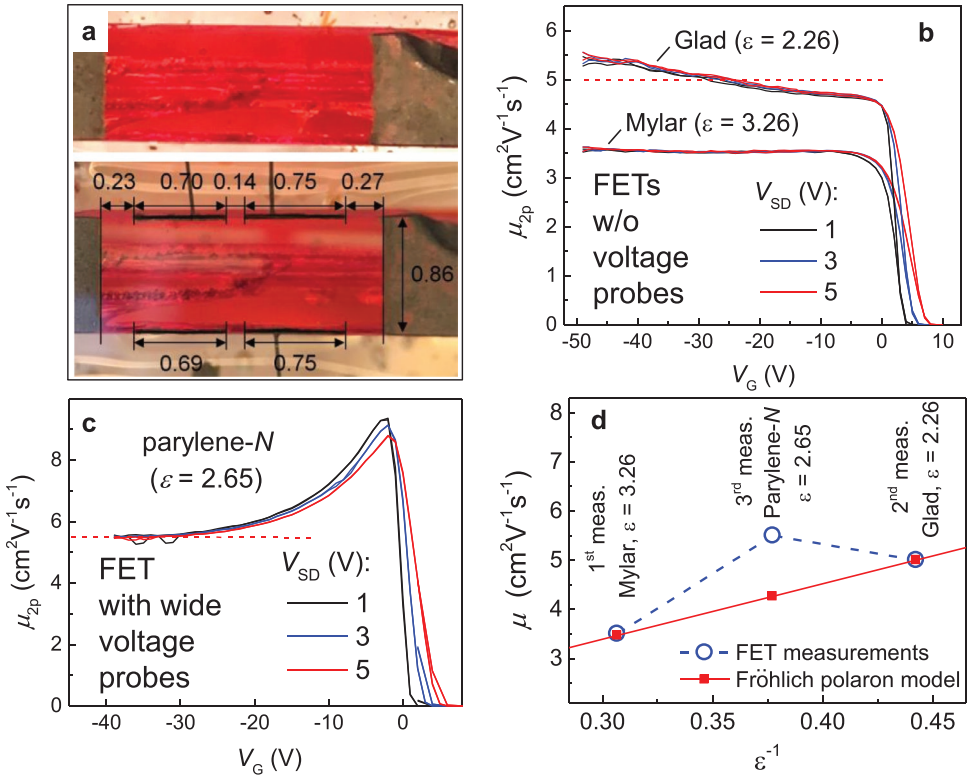

Figure 4. Experimental demonstration of longitudinal channel shunting in single-crystal OFETs. a) Photographs of a rubrene single crystal with graphite source and drain contacts (upper) and the same crystal after the intentionally wide voltage probes were added (lower). The dimensions are indicated in millimeters. b) FET mobilities measured on a clean crystal without the voltage probes by using vacuum-laminated Mylar and Glad gate dielectrics. c) FET mobility measured on the same single crystal, but with wide voltage probes added in the channel and a parylene-N gate insulator. The corresponding ε values of all the gate dielectrics are indicated in parenthesis. d) Comparison of the carrier mobilities expected from the Fröhlich polaron theory, $\mu \propto \varepsilon^{-1}$ (red solid squares), with the experimental μ values (blue open circles). While the devices without the voltage probes agree with the expected $\mu(\varepsilon)$ dependence, the device with the wide voltage probes shows an overestimated mobility. In this experiment, crystal-to-crystal variations are avoided, thanks to the vacuum lamination technique that allows using the same single crystal in all the three measurements.

significantly overestimated. Figure 3 can be used as a "conversion table:" by looking up a specific α value, corresponding to a given device geometry (t/D and L/W), the conventional 4-probe experimental mobility can be converted to the correct mobility by using Equation (9). An additional plot in the Supporting Information gives a blow-up view of these data for $0 \le t/D \le 0.4$, where most of the experimental devices would reside (Figure S2, Supporting Information). Although here we only present the results for the type of 4-probe geometry with an even division of the channel into three equal sections ($D = L/3$), we include a downloadable Mathematica code used in these simulations that can be easily modified to accommodate other structures (Supporting Information).

4. Experimental Evaluation of Longitudinal Channel Shunting in 4-Probe OFETs

To study longitudinal channel shunting experimentally and compare the results with numerical simulations, we first prepare single-crystal OFETs with and without voltage probes in the channel (**Figure 4**). High-quality vapor grown rubrene ($C_{42}H_{28}$) single crystals were used as the organic semiconductor, and a colloidal graphite (carbon paint) was used for the source–drain contacts and voltage probes.[11,25] As gate insulators, we used several materials with different dielectric permittivities, ε, including commercially available freestanding Mylar ($\varepsilon = 3.26$) and Glad ($\varepsilon = 2.26$) films,[26] as well as vapor-grown parylene-N ($\varepsilon = 2.65$).[11] To avoid errors caused by crystal-to-crystal variations, we have designed an experiment, in which the same rubrene single crystal could be used in a combination with different gate dielectrics sequentially applied to the crystal surface by the vacuum lamination technique.[26] This technique allows repeated applications of different dielectric films, as well as multiple FET measurements, performed on the same crystal without damaging the surface. As our 1st and 2nd steps, we have prepared a pristine device ($L/W = 2.4$) without any voltage probes (the upper photograph in Figure 4a) and measured the 2-probe linear-regime carrier mobilities μ_{2p} by sequentially laminating Mylar and Glad gate dielectrics. These FET measurements yielded the average (over the plateau) mobilities of $\mu_{2p} = 3.5$ and 5 cm^2 V^{-1} s^{-1} for Mylar and Glad, respectively (Figure 4b). As the 3rd step, after delaminating the gate polymer films from the crystal, we have deposited wide voltage probes on the sides of the channel, yielding $D/W = 1$ and $t/D = 0.83$ (the lower photograph in Figure 4a). With these voltage probes and wires attached to them, reliable vacuum lamination of dielectric membranes is no longer possible, and thus we have used parylene conformal coating to create a new

FET: the sample was coated with parylene-N, followed by evaporation of Ag gate. This FET's mobility in the linear regime was $\mu_{2p} = 5.5$ cm^2 V^{-1} s^{-1} (Figure 4c).

The analysis of these three measurements confirms that a longitudinal channel shunting takes place in the device with wide voltage probes. According to the interfacial (Fröhlich) polaron model, charge carrier mobility at semiconductor–insulator interfaces is inversely proportional to the dielectric permittivity of the gate insulator: $\mu = \varepsilon^{-1} \cdot \mu_0$.[26–28] This behavior occurs in our measurements of the pristine devices (those that do not have voltage probes in the channel) labeled as 1st and 2nd measurement in Figure 4d. Indeed, the relative difference in mobilities between these two data points match the expectation based on the Fröhlich polaron model for the corresponding ε values. On the contrary, the device with wide voltage probes has an apparent mobility of $\mu_{2p} = 5.5$ cm^2 V^{-1} s^{-1}, significantly exceeding its mobility of 4.25 cm^2 V^{-1} s^{-1} expected from the ε^{-1} dependence (the data point labeled "3rd meas." in Figure 4d). This increase of mobility in the FET with wide voltage probes is consistent with the channel shunting effect.

To evaluate the effect more quantitatively, we have performed 4-probe measurements of the FET with the wide voltage probes ($t = 0.72$ mm and $t/D = 0.83$, the contact layout shown in the lower portion of Figure 4a). For the detailed 4-probe measurements, see Figure S3 (Supporting Information). These measurements confirm that substantial channel shunting not only leads to overestimated mobilities, μ_{2p} and μ_{4p}, but can also result in a less accurate evaluation of contact resistance (**Figure 5**). It is well known that rubrene single-crystal OFETs with graphite contacts and long channels (here, $L \approx 2.1$ mm) have rather low relative contact resistance, which allows for an efficient hole injection and typically leads to matching true 4-probe and 2-probe mobilities ($\mu_{4p\text{-corr}}/\mu_{2p\text{-corr}} \approx 1$) (see refs. [4,20] and Figure S4a (Supporting Information)). Figure 5 shows the conventional 2-probe and 4-probe mobilities extracted from these measurements. Since all the contacts were made using carbon paint, we normally expect to see the matching μ_{2p} and μ_{4p}. On the contrary, Figure 5 reveals that μ_{4p} is systematically higher than μ_{2p} (with the ratio $\mu_{2p}/\mu_{4p} \approx 0.77$) even at the highest gate voltage $V_G = -40$ V, when the Schottky barriers are expected to be fully suppressed. Judging by this ratio alone, one would draw a conclusion that contact resistance of the device in Figure 5 is substantial, which is not actually the case. This behavior is consistent with the model described above (Equation (6)), which predicts that for $D/L < 0.5$ (in this device, $D/L = 0.42$), the ratio of conventional mobilities $k = \mu_{2p}/\mu_{4p} < 1$ and would thus overestimate the severity of the contact resistance problem. This measurement not only confirms the longitudinal shunting effect, but also highlights the importance of taking it into account in evaluation of contact resistance in 4-probe measurements.

To obtain more quantitative comparison, we ran numerical simulations for this device using the same code as that used in Figures 2 and 3, but now with $D/L = 0.42$ (Figure S5, Supporting Information). The modeling suggests that conventional 4-probe mobility of this device would be overestimated by 96% ($\alpha = 1.96$) due to the very wide voltage probes. The experiment indeed shows that μ_{4p} is greater than the true mobility of this device by a factor of 1.79 (Figure 5).

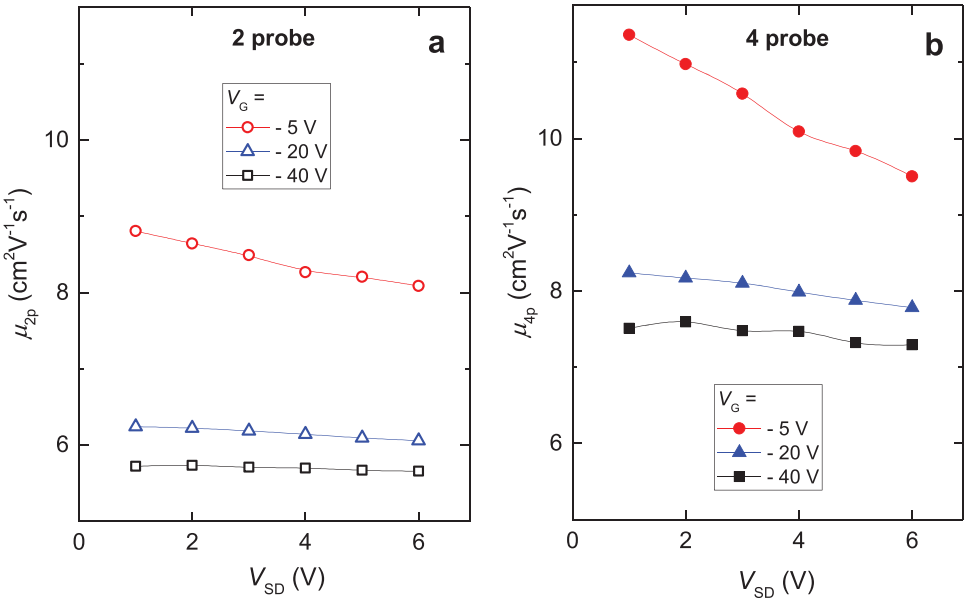

Figure 5. a,b) Comparison of the conventional (not corrected for shunting) μ_{2p} and μ_{4p} mobility measurements in a rubrene single-crystal OFET with very wide voltage probes. The contact structure is shown in the lower photograph in Figure 4a. The gate dielectric is parylene-N ($\varepsilon = 2.65$). The mobilities are calculated by using the conventional Equations (1) and (4). Measurements are performed at $V_G = -5$ V (circles), –20 V (triangles), and –40 V (squares). Because the contact resistance in this type of OFETs is negligible in comparison with the channel resistance, the expected ratio μ_{4p}/μ_{2p} is 1. The apparent ratio, however, is systematically higher, $\mu_{4p}/\mu_{2p} \approx 1.3$, irrespective of V_G and V_{SD}, due to the longitudinal channel shunting effect. The apparent 4-probe mobility is μ_{4p} ($V_G = -40$ V) ≈ 7.6 cm^2 V^{-1} s^{-1} (panel (b)), that is, greater than the true mobility of 4.25 cm^2 V^{-1} s^{-1} (Figure 4) by a factor $\alpha = 1.79$, which is close to the prediction of the numerical simulations for this device (Figure S5, Supporting Information).

In addition to single-crystal OFETs, we have also investigated this effect in organic thin-film transistors (OTFT), in which more straightforward evaluation of mobility overestimation due to channel shunting can be made. In this part, we first optimized a blend of small molecule 2,7-dioctyl[1]benzothieno[3,2-b][1]benzothiophene (C_8-BTBT)[29] with the indacenodithiophene-benzothiadiazole conjugated copolymer (C_{16}IDT-BT),[30] the so-called C_8-BTBT:C_{16}IDT-BT blend. OTFTs based on blends have just started to emerge, showing potential for film processability and achieving high-μ devices.[30,31] However, the initial results raise many important questions as of the intrinsic carrier mobility in such blends, the degree of phase inhomogeneity and phase separation occurring in the blends, crystalline order versus disorder, grain size and morphology, and how all these factors affect μ. Since few existing studies only used 2-probe FETs, and no Hall effect measurements were performed in blended OFETs, it becomes essential to carry out these measurements.

The optimized blend (see the Experimental Section) was spin coated on glass substrates with sputtered Pt/Ti contacts, followed by a thermal annealing and deposition of a parylene-N gate dielectric. Transparent indium tin oxide (ITO) gate electrode was sputtered on top (for details on optimized fabrication, see the Experimental Section). The resultant devices are polycrystalline OTFT in a bottom-contact/top-gate architecture. Prior to FET fabrication, crystallized blends were characterized via a polarized optical microscopy and an atomic force microscopy (AFM) that revealed a polycrystalline morphology of these films with ≈100 µm sized C_8-BTBT grains (**Figure 6**a) and molecularly flat terraces with 1.5 nm high steps, consistent with packing of C_8-BTBT molecules (Figure 6b). These data confirm that a vertical phase separation takes place in the blends, with C_8-BTBT crystallizing on top of the film (for more details, see Figure S6 in the Supporting Information).

To investigate the shunting effect, here we propose an unconventional contact geometry (Figure 6c), in which voltage probes of varied width t (labeled 1–4) are incorporated symmetrically along both sides of the channel at even center-to-center distances. This structure allows for both

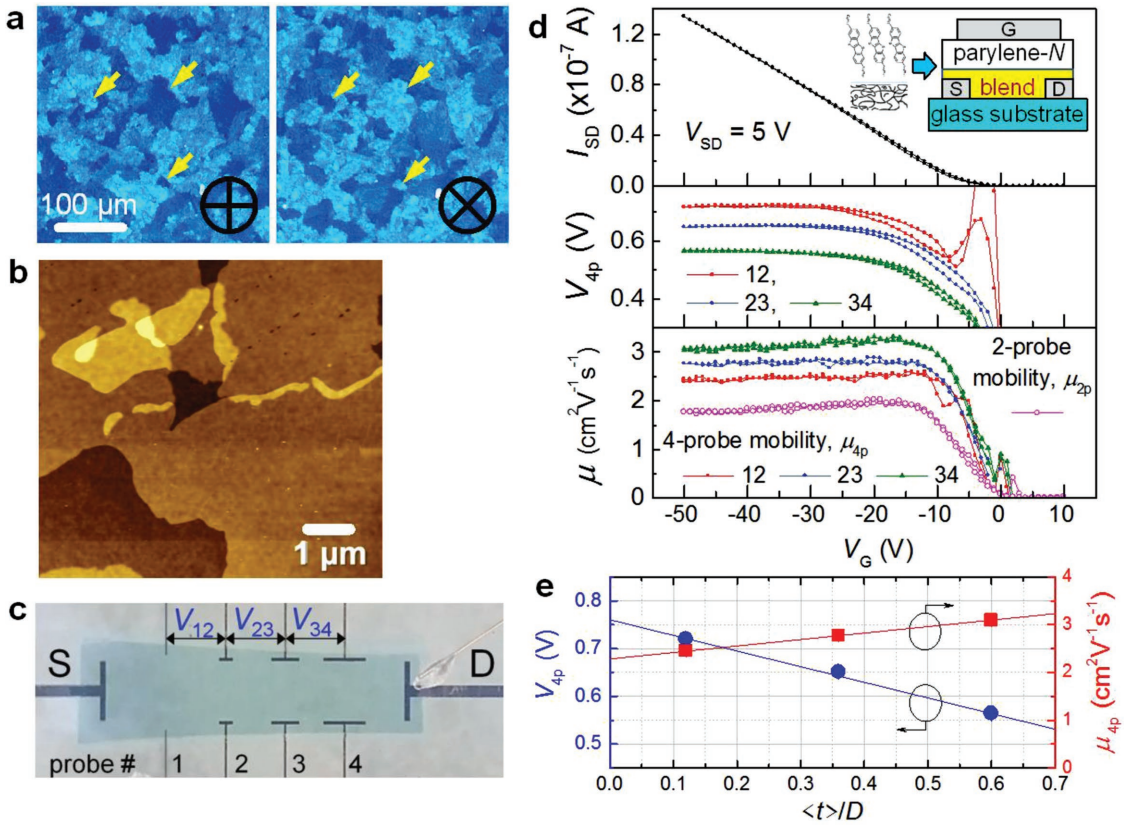

Figure 6. Experimental demonstration of longitudinal channel shunting in the polycrystalline OTFT based on C_8-BTBT:C_{16}IDT-BT blend. a) Polarized optical microscope images of a crystallized blend, showing a contrast inversion in polycrystalline domains. b) AFM surface morphology of the film, showing C_8-BTBT terraces and 1.5 nm high steps (see also Figure S6 in the Supporting Information). c) A photograph of a FET with multiple voltage/Hall probes of a varied width, $t_1 = 5$ µm, $t_2 = 120$ µm, $t_3 = 240$ µm, and $t_4 = 360$ µm. The center-to-center distance between the adjacent probes along the channel $D = 0.5$ mm, $L = 2.5$ mm, and $W = 0.5$ mm. d) Top: transfer curve of the OTFT in the linear regime ($V_{SD} = 5$ V, V_G sweep rate is 1 V s^{-1}). The inset schematically shows the device structure. Middle: 4-probe voltages V_{4p} measured between the adjacent voltage probes, labeled "12," "23," and "34." Bottom: the corresponding conventional (not corrected for shunting) mobilities μ_{4p} (and μ_{2p}) obtained by using V_{4p} (and V_{SD}) via Equation (1) (and Equation (4)). e) V_{4p} and μ_{4p} as functions of the relative width of the voltage probes $\langle t \rangle / D$. The mobility values in panel (e) correspond to the plateau at high $V_G = -50$ V in panel (d), and $\langle t \rangle$ is calculated as $(t_i + t_{i+1})/2$, for $i = 1, 2, 3$. It is evident that with increasing voltage probe width, the 4-probe voltage becomes increasingly underestimated, while the 4-probe mobility increasingly overestimated.

4-probe and Hall effect measurements to be performed in the same transistor as a function of varied probe width t. The potential drops along the channel between each pair of neighboring voltage probes, labeled in Figure 6d as V_{12}, V_{23}, and V_{34}, are monitored in situ during the FET measurements and used as V_{4p} in the calculation of 4-probe mobility μ_{4p} as per the conventional formula (Equation (1)). Except for the probe width t, all the other device parameters and measurement conditions, including V_{SD}, V_G, I_{SD}, W, C_i, and D, are the same for all the probe pairs. Thus, a measurement like this would normally be expected to yield similar voltage drops V_{4p} for all the pairs, assuming that the longitudinal shunting can be ignored. Values of V_{4p} and μ_{4p} for all the three pairs of adjacent voltage probes are plotted in Figure 6e as a function of average probe width $\langle t_i \rangle = (t_i + t_{i+1})/2$, $i = 1$, 2, 3. It can be clearly seen that V_{4p} systematically decreases with an increasing probe width, as we go along the channel from left to right, leading to the 4-probe mobility computed by conventional Equation (1) to increase with increasing $\langle t_i \rangle$ (Figure 6e). This observation directly points to the longitudinal channel shunting that leads to an overestimated μ_{4p}. A tendency of V_{4p} to decrease linearly with $\langle t \rangle$ suggests that a linear extrapolation of these data to $\langle t \rangle = 0$ could be used to estimate a shunt-corrected 4-probe carrier mobility. In this OTFT, this value is $\mu_{4p\text{-}corr} = 2.3$ cm^2 V^{-1} s^{-1}, which is within the typical spread of statistical distribution of μ for undoped C_8-BTBT:C_{16}IDT-BT blends.[30,32]

5. Longitudinal Channel Shunting and Hall Effect Measurements

Hall effect measurements use Hall voltage probes on the opposite sides of the channel (**Figure 7**). The Hall voltage, V_H, measured between the Hall probes originates from a transverse Lorentz force acting on charge carriers, as they drift along the channel.[14,15,19] Here, we observed that the measured Hall voltage systematically decreases with the width of the Hall probes (Figure 7a). The same polycrystalline OTFT as in Figure 6, with four pairs of Hall probes of different width, was used in these Hall measurements, which were carried out by using a high-resolution AC-Hall effect technique (for details, see ref. [20] and Figure S7 in the Supporting Information). Figure 7a shows V_H and μ_H as functions of the relative width t/D of the Hall probes. Hall mobility $\mu_H \equiv \sigma_{4p}/(en_H)$ has been calculated by the conventional formula (Equation (7)).[19] The observation of a Hall voltage V_H decreasing with t/D clearly suggests that Lorentz force, F_L, acting on charge carriers flowing between the Hall probes is weakened by the reduced longitudinal drift velocity in this region. Indeed, the device modeling clearly shows that the longitudinal electric field (and thus the drift velocity) is reduced in the region between the Hall probes (Figure 2). In addition, the distribution of the longitudinal component of the electric field (and drift velocity) over the width of the channel in this region has a maximum at the center of the channel and minima near both edges of the Hall probes (Figure 7b), which

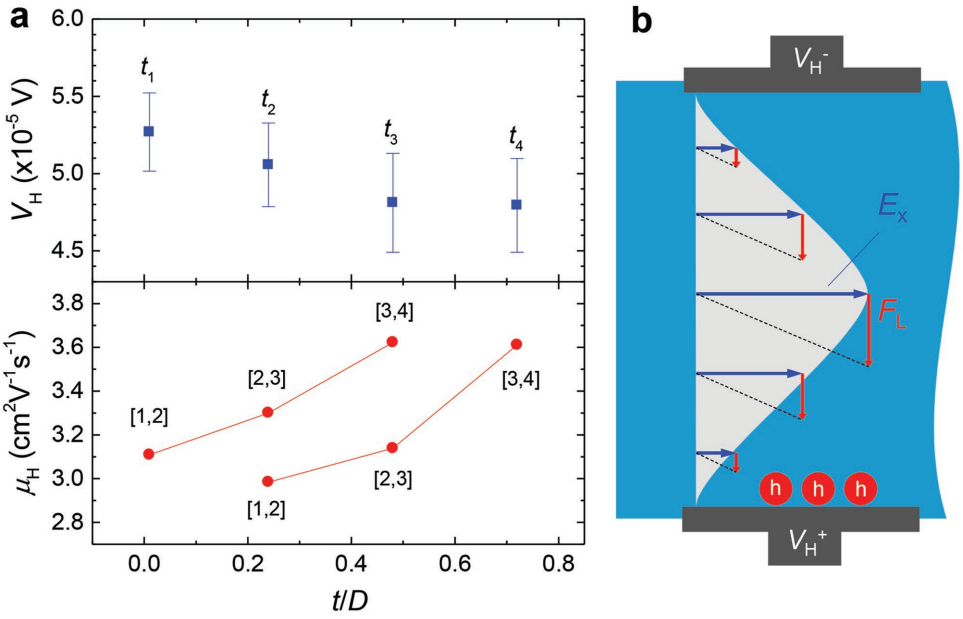

Figure 7. The effect of longitudinal channel shunting on Hall measurements in the polycrystalline OTFT based on C_8-BTBT:C_{16}IDT-BT blend. a) Measured Hall voltage (upper panel) and Hall mobility (lower panel), V_H and μ_H, as functions of the relative width of the Hall probes, t/D. The same device as that shown in Figure 6a was used. Measurements were performed at $V_G = -50$ V, $V_{SD} = 5$ V, and $I_{SD} = 126$–130 nA via a high-resolution AC-Hall effect methodology ($B_{rms} = 0.2314$ T, frequency $f = 0.7$ Hz).[20] The Hall mobility μ_H is determined by Equation (7), in which V_H is the Hall voltage measured between each pair of Hall probes (corresponding to the probe widths t_1, t_2, t_3, and t_4), and V_{4p} is the longitudinal 4-probe voltage drop measured between the pairs of adjacent probes (various probe combinations used for V_{4p} in μ_H calculations are indicated as [i,j]). b) An illustration of the effect of Lorentz force reduction due to the longitudinal channel shunting: equipotential edges of the Hall probes result in a lower longitudinal electric field E_x and a reduced drift velocity for carriers passing between the Hall probes. This effect is especially strong in the vicinity of the probe edges, thus resulting in a smaller average Lorentz force, F_L, and a reduced measured Hall voltage, V_H. For the raw AC-Hall measurement data, see Figure S7 (Supporting Information).

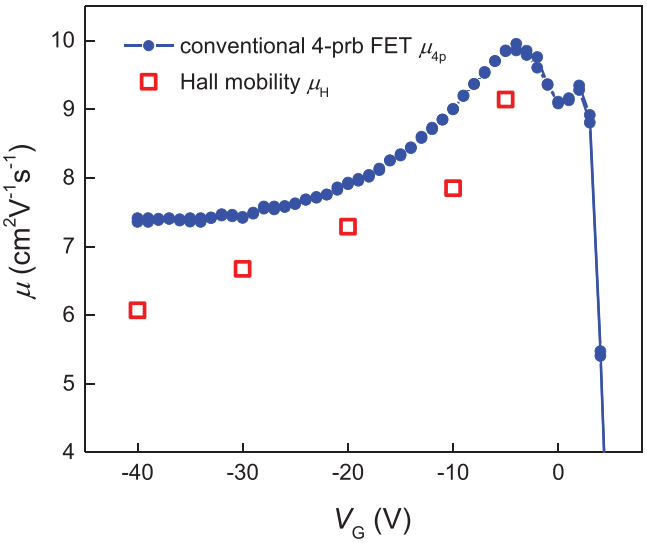

Figure 8. Comparison of the longitudinal 4-probe and Hall mobility measurements in a pristine rubrene single-crystal OFET with voltage/Hall probes of substantial width. The same device as in Figure 5 and Figure S3 (Supporting Information) is used (the contact layout is shown in the lower photograph in Figure 4a). Instead of the typical for these devices "fully developed" Hall effect (that is, $\mu_H = \mu_{4p}$), the data apparently suggest that Hall effect is "underdeveloped" ($\mu_H < \mu_{4p}$). Such a behavior could be misinterpreted as being caused by a significant hopping contribution to the charge transport, if the notion of longitudinal channel shunting is not taken into account. For the raw AC-Hall measurement data, see Figure S8 (Supporting Information).

is opposite to the tendency observed at the midline (compare with Figure 2c). This effect, imposed by the equipotential edges of the Hall probes, results in a reduced F_L and V_H, thus leading to an overestimated Hall carrier density n_H, especially noticeable in devices with Hall probes of substantial width. We note, however, that experimental μ_H shows a trend different from that of V_H (Figure 7a), because the calculation of μ_H also uses the overestimated longitudinal conductivity σ_{4p} (Equation (7)).

An additional demonstration of differences between Hall and longitudinal mobility measurements occurring in FETs with wide voltage probes is shown in **Figure 8**. Here, μ_{4p} and μ_H measurements (neither corrected for shunting) were carried out in pristine rubrene single-crystal OFET with relatively wide voltage and Hall probes (for the raw AC-Hall data, see Figure S8 in the Supporting Information). It can be clearly seen that $\mu_H < \mu_{4p}$, which is uncommon for pristine rubrene OFETs that typically exhibit a fully coherent (or, the so-called fully developed) Hall effect with $\mu_{4p} = \mu_H$.[14–16,19] The reason that $\mu_H < \mu_{4p}$ in this case is because the calculation $\mu_H \equiv \sigma_{4p}/(en_H)$ relies on σ_{4p} and n_H that are both overestimated, while the calculation $\mu_{4p} = C_i^{-1} \cdot d\sigma_{4p}/dV_G$ only relies on the overestimated σ_{4p}. An underdeveloped Hall effect ($\mu_H < \mu_{4p}$) can occur in certain systems,[17,18,33,34] where hopping and band-like carriers coexist, and the hopping component substantially contributes to the charge transport, leading to a noticeable Hall voltage compensation effect with $\mu_H < \mu_{4p}$.[19] However, such an interpretation of the behavior shown in Figure 8 would be inconsistent with the fact that the studied device is a pristine rubrene FET. Without the knowledge of longitudinal channel shunting, one could wrongfully interpret the data in Figure 8 as the evidence of a significant hopping in the system, which is clearly not the case in these devices.

6. Conclusions

We have carried out a combination of numerical simulations, FET measurements, and Hall effect studies in single-crystal and polycrystalline blended OFETs showing that charge carrier transport measurements in 4-probe contact geometry could suffer from a significant mobility overestimation caused by longitudinal channel shunting. This effect, imposed by equipotential edges of voltage probes, is especially noticeable in FETs with long but narrow channels (elongated channel geometry) and voltage probes of substantial widths. In such devices, conventional 4-probe data analysis could lead to mobilities overestimated by as much as ≈350%. We introduced a conversion factor, based on numerical simulations, that can be used to obtain the correct mobility from conventional 4-probe experimental data. We also show that longitudinal channel shunting influences Hall voltage measurements and may thus lead to errors in Hall mobility. These demonstrations are critical for the correct quantitative analysis of charge carrier transport in a variety of emergent electronic materials and devices, including those based on organic semiconductors, inorganic oxides, monolayer materials, as well as nanostructured semiconductors such as carbon nanotube or nanowire meshes and nanocrystal arrays. This work shows that in devices, where technical constrains do not allow drastically reducing the width of the voltage probes, corrections of conventional 4-probe mobility for the shunting errors are necessary.

7. Experimental Section

Fabrication of Rubrene Single-Crystal FETs: Top-gate, top-contact FETs were fabricated at the (*a*,*b*) facets of pristine rubrene single crystals grown in a stream of ultrahigh purity (UHP) Ar by physical vapor transport.[35] The contacts were hand-painted under a microscope with an aqueous suspension of colloidal graphite (Ted Pella #16051).[25] Commercially available plastic membranes (2.5 µm thick biaxially oriented Mylar (Chemplex, Cat. No. 100), and 11 µm thick low-density polyethylene or "Glad" for food wrapping (Walmart)) were vacuum-laminated as gate dielectrics.[26] Parylene-N was grown in a custom-designed parylene reactor from a dimer precursor purchased at Specialty Coating Systems (for details, see ref. [10] and technical notes at the group's website[25]). Parylene-N thickness was 1.15 µm, yielding a gate–channel capacitance $C_i = 2.04$ nF cm^{-2}, confirmed by capacitance-voltage (CV) measurements at 60 Hz–1 MHz.[25] For gate electrodes, a thermally evaporated silver or silver paint (Ted Pella #16032) was used on Parylene-N and the plastic membranes, respectively.

Fabrication of Polycrystalline OTFTs: Top-gate, bottom-contact FETs were fabricated on glass substrates that were sequentially cleaned in a detergent solution (DECON 90, 1% diluted in deionized water), acetone, and isopropanol. For the contacts, 2 nm thick Ti adhesion layer was deposited on glass first, followed by 20 nm thick Pt, both sputtered through a contact shadow mask by a DC magnetron sputtering in 5 mTorr of UHP Ar. Channel length and width were $L = 2.5$ mm and $W = 0.5$ mm, and the center-to-center distance between the neighboring voltage probes was $D = 0.5$ mm. For polycrystalline organic semiconductor films, a blended solution of C_8-BTBT molecules and C_{16}IDT-BT conjugated copolymer (ratio C_8-BTBT:C_{16}IDT-BT = 1:4) at 10 mg mL^{-1} concentration in a mixture of tetralin and chlorobenzene solvents (ratio 1:1) was first prepared. The blend was deposited from a solution heated to 60 °C onto

the substrates via spin coating in nitrogen atmosphere. Following spin coating, the film was postannealed by placing the sample on a hotplate for 5 min at 120 °C.[30] Next, a 1.43 µm thick parylene-N layer was grown on top of the C_8-BTBT:C_{16}IDT-BT blend, yielding a gate–channel capacitance $C_i = 1.64$ nF cm^{-2}. The FET structure was then completed by a 50 nm thick ITO gate sputtered through a shadow mask.

Polarized Optical Microscopy: A Nikon LV-100 microscope was used to obtain optical imaging for the C_8-BTBT:C_{16}IDT-BT blend semiconductor.

Atomic Force Microscopy: Topographical information for the C_8-BTBT:C_{16}IDT-BT blend semiconductor was gathered using an Agilent 5500 scanning probe, operating in tapping mode. Further image analysis was undertaken using Gwyddion 2.39.

FET and Hall Effect Measurements: All the electrical measurements were performed at room temperature. Keithley Source Meters K2400 and Electrometers K6512 were used for FET measurement. V_G sweep rate in FET measurements was 0.5–1 V s^{-1}. The AC-Hall effect measurements were carried out following the previously reported methodology.[20] An AC magnetic field of frequency 0.55–0.7 Hz and root-mean-square (rms) magnitude $B_{rms} = 0.2314$ T were generated by a rotating assembly of permanent Nd magnets. In-phase and out-of-phase Hall voltage signals, ΔV_H^{iP} and ΔV_H^{oP}, were detected by a lock-in amplifier tuned in the frequency of the oscillating magnetic field (Supporting Information). The Hall voltage, V_H, used in Hall mobility calculations was determined as $V_H = [(\Delta V_H^{iP})^2 + (\Delta V_H^{oP})^2]^{1/2}$.

Supporting Information

Supporting Information is available from the Wiley Online Library or from the author.

Acknowledgements

The authors are grateful to the following programs for the financial support of this work: the National Science Foundation under the grant DMR-1506609, the Rutgers Energy Institute (REI), the Center for Advanced Soft-Electronics funded by the Ministry of Science, ICT and Future Planning as Global Frontier Project (CASE-2011-0031628), and the Ministry of Education and Science of the Russian Federation in the framework of Increase Competitiveness Program of NUST «MISiS» (№ K3-2016-004), implemented by a governmental decree dated 16th of March 2013, N 211. T.D.A., and A.F.P, acknowledge the King Abdullah University of Science and Technology (KAUST) for financial support.

Conflict of Interest

The authors declare no conflict of interest.

Keywords

conjugated polymers, field-effect transistors, mobility, molecular crystals, organic semiconductors

Received: December 6, 2017
Revised: March 4, 2018
Published online:

[1] C. H. Ahn, A. Bhattacharya, M. Di Ventra, J. N. Eckstein, C. D. Frisbie, M. E. Gershenson, A. M. Goldman, I. H. Inoue, J. Mannhart, A. J. Millis, A. F. Morpurgo, D. Natelson, J.-M. Triscone, *Rev. Mod. Phys.* **2006**, *78*, 1185.
[2] H. H. Choi, K. Cho, C. D. Frisbie, H. Sirringhaus, V. Podzorov, *Nat. Mater.* **2018**, *17*, 2.
[3] S. M. Sze, K. K. Ng, *Physics of Semiconductor Devices*, John Wiley & Sons **2006**.
[4] V. Podzorov, *MRS Bull.* **2013**, *38*, 15.
[5] Z. Bao, J. Locklin, *Organic Field-Effect Transistors*, CRC Press **2007**.
[6] D. Natali, M. Caironi, *Adv. Mater.* **2012**, *24*, 1357.
[7] V. Podzorov, M. E. Gershenson, C. Kloc, R. Zeis, E. Bucher, *Appl. Phys. Lett.* **2004**, *84*, 3301.
[8] D. Cahen, A. Kahn, E. Umbach, *Mater. Today* **2005**, *8*, 32.
[9] R. Martel, V. Derycke, C. Lavoie, J. Appenzeller, K. K. Chan, J. Tersoff, P. Avouris, *Phys. Rev. Lett.* **2001**, *87*, 256805.
[10] V. Podzorov, V. M. Pudalov, M. E. Gershenson, *Appl. Phys. Lett.* **2003**, *82*, 1739.
[11] V. Podzorov, S. E. Sysoev, E. Loginova, V. M. Pudalov, M. E. Gershenson, *Appl. Phys. Lett.* **2003**, *83*, 3504.
[12] J. Takeya, C. Goldmann, S. Haas, K. P. Pernstich, B. Ketterer, B. Batlogg, *J. Appl. Phys.* **2003**, *94*, 5800.
[13] C. R. Newman, R. J. Chesterfield, J. A. Merlo, C. D. Frisbie, *Appl. Phys. Lett.* **2004**, *85*, 422.
[14] V. Podzorov, E. Menard, J. A. Rogers, M. E. Gershenson, *Phys. Rev. Lett.* **2005**, *95*, 226601.
[15] J. Takeya, K. Tsukagoshi, Y. Aoyagi, T. Takenobu, Y. Iwasa, *Jpn. J. Appl. Phys.* **2005**, *44*, L1393.
[16] W. Xie, S. Wang, X. Zhang, C. Leighton, C. D. Frisbie, *Phys. Rev. Lett.* **2014**, *113*, 246602.
[17] S. Wang, M. Ha, M. Manno, C. D. Frisbie, C. Leighton, *Nat. Commun.* **2012**, *3*, 1210.
[18] Y. Yamashita, F. Hinkel, T. Marszalek, W. Zajaczkowski, W. Pisula, M. Baumgarten, H. Matsui, K. Müllen, J. Takeya, *Chem. Mater.* **2016**, *28*, 420.
[19] H. T. Yi, Y. N. Gartstein, V. Podzorov, *Sci. Rep.* **2016**, *6*, 23650.
[20] Y. Chen, H. T. Yi, V. Podzorov, *Phys. Rev. Appl.* **2016**, *5*, 034008.
[21] S. P. Senanayak, A. Z. Ashar, C. Kanimozhi, S. Patil, K. S. Narayan, *Phys. Rev. B* **2015**, *91*, 115302.
[22] J. Jang, W. Liu, J. S. Son, D. V. Talapin, *Nano Lett.* **2014**, *14*, 653.
[23] N. A. Minder, S. Ono, Z. Chen, A. Facchetti, A. F. Morpurgo, *Adv. Mater.* **2012**, *24*, 503.
[24] K. Nagashio, T. Nishimura, K. Kita, A. Toriumi, *Appl. Phys. Lett.* **2010**, *97*, 143514.
[25] Technical notes at Podzorov group's page, http://www.physics.rutgers.edu/~podzorov/ (accessed: April 2018).
[26] H. T. Yi, Y. Chen, K. Czelen, V. Podzorov, *Adv. Mater.* **2011**, *23*, 5807.
[27] I. N. Hulea, S. Fratini, H. Xie, C. L. Mulder, N. N. Iossad, G. Rastelli, S. Ciuchi, A. F. Morpurgo, *Nat. Mater.* **2006**, *5*, 982.
[28] J. Veres, S. D. Ogier, S. W. Leeming, D. C. Cupertino, S. Mohialdin Khaffaf, *Adv. Funct. Mater.* **2003**, *13*, 199.
[29] T. Uemura, K. Nakayama, Y. Hirose, J. Soeda, M. Uno, W. Li, M. Yamagishi, Y. Okada, J. Takeya, *Curr. Appl. Phys.* **2012**, *12*, S87.
[30] A. F. Paterson, N. D. Treat, W. Zhang, Z. Fei, G. Wyatt-Moon, H. Faber, G. Vourlias, P. A. Patsalas, O. Solomeshch, N. Tessler, M. Heeney, T. D. Anthopoulos, *Adv. Mater.* **2016**, *28*, 7791.
[31] J. Panidi, A. F. Paterson, D. Khim, Z. Fei, Y. Han, L. Tsetseris, G. Vourlias, P. A. Patsalas, M. Heeney, T. D. Anthopoulos, *Adv. Sci.* **2018**, *5*, 1700290.
[32] A. F. Paterson, Y.-H. Lin, A. D. Mottram, Z. Fei, M. R. Niazi, A. R. Kirmani, A. Amassian, O. Solomeshch, N. Tessler, M. Heeney, T. D. Anthopoulos, *Adv. Electron. Mater.* **2017**, 1700464, https://doi.org/10.1002/aelm.201700464.
[33] T. Uemura, M. Yamagishi, J. Soeda, Y. Takatsuki, Y. Okada, Y. Nakazawa, J. Takeya, *Phys. Rev. B* **2012**, *85*, 035313.
[34] J.-F. Chang, T. Sakanoue, Y. Olivier, T. Uemura, M.-B. Dufourg-Madec, S. G. Yeates, J. Cornil, J. Takeya, A. Troisi, H. Sirringhaus, *Phys. Rev. Lett.* **2011**, *107*, 066601.
[35] M. E. Gershenson, V. Podzorov, A. F. Morpurgo, *Rev. Mod. Phys.* **2006**, *78*, 973.